



Ferroelectricity from spin supercurrents in LiCuVO₄

M. Mourigal,^{1,2} M. Enderle,¹ R. K. Kremer,³ J. M. Law,³ and B. Fåk⁴

¹Institut Laue-Langevin, BP156, F-38042 Grenoble Cedex 9, France

²Laboratory for Quantum Magnetism, École Polytechnique Fédérale de Lausanne (EPFL), CH-1015 Lausanne, Switzerland

³Max-Planck Institute for Solid State Research, Heisenbergstrasse 1, D-70569 Stuttgart, Germany

⁴Commissariat à l'Énergie Atomique, INAC, SPSMS, F-38054 Grenoble, France

(Received 21 December 2010; revised manuscript received 1 March 2011; published 22 March 2011)

We have studied the magnetic structure of the ferroelectric frustrated spin-1/2 chain material LiCuVO₄ in applied electric and magnetic fields using polarized neutrons. A symmetry and mean-field analysis of the data rules out the presence of static Dzyaloshinskii-Moriya interaction, while exchange striction is shown to be negligible by our specific-heat measurements. The experimentally observed magnetoelectric coupling is in excellent agreement with the predictions of a purely electronic mechanism based on spin supercurrents.

DOI: 10.1103/PhysRevB.83.100409

PACS number(s): 75.10.Jm, 77.80.-e, 75.10.Pq, 71.70.Ej

Materials where ferroelectricity (FE) appears simultaneously with magnetic order are referred to as type-II or magnetic multiferroics. Considerable attention has been devoted to their unconventional magnetoelectric (ME) effects,¹ namely the control of their electric polarization \mathbf{P} with an external magnetic field \mathbf{H} ,² and likewise at $H = 0$ the favoring of a particular magnetic domain by an applied electric field \mathbf{E} .³⁻⁷ However, the fundamental mechanisms responsible for FE in this class of materials are under debate, in particular whether FE always results from atomic displacements or whether it can be induced by a purely electronic mechanism based on spin supercurrents⁸ via the Aharonov-Casher effect, a relativistic topological quantum effect for neutral magnetic particles. Here, like in the spin Hall effect,⁹ the electric field directly controls the spin current without intermediating atomic displacements.

Phenomenologically, a spin spiral may induce an electric polarization $\mathbf{P} = A\mathbf{e}_{12} \times (\mathbf{S}_1 \times \mathbf{S}_2)$, where \mathbf{e}_{12} links neighboring spin sites \mathbf{S}_1 and \mathbf{S}_2 and A depends on the fundamental mechanism of the ME coupling.¹⁰ Mechanisms that are experimentally established involve symmetry-breaking lattice distortions, which are either induced by symmetric exchange¹¹ or by asymmetric Dzyaloshinskii-Moriya interaction (DMI).^{12,13} The spin supercurrent mechanism,⁸ on the other hand, operates in the absence of magnetostriction and static DMI. Here frustration of the symmetric exchange interactions leads to noncollinear magnetic order and a spin supercurrent that couples to the electric field via the relativistic spin-orbit coupling (SOC). The sign and size of A is therefore materials specific.^{8,14} However, the spin supercurrent *vanishes* if the spin spiral is stabilized by DMI,⁸ and the latter is present in many materials, e.g. those studied in Refs. 4-7.

In this Rapid Communication, we provide strong experimental evidence that the ferroelectricity in the frustrated spin-1/2 chain material LiCuVO₄ is purely driven by the spin supercurrent mechanism,^{8,14} and that magnetostriction is negligible. By combining mean-field theory and symmetry analysis with polarized neutron-diffraction measurements of the magnetic structure in crossed electric and magnetic fields, we show that the static DMI plays no role in driving LiCuVO₄ to a spin-spiral ferroelectric state.

LiCuVO₄ crystallizes in the orthorhombic *Imma* space group (#74), where the two Cu²⁺ ions in the primitive

unit cell are located at the positions $\mathbf{r}_1 = (0,0,0)$ and $\mathbf{r}_2 = (0,1/2,0)$ [Fig. 1(a)]. They form spin-1/2 chains along the b axis built up from edge-sharing CuO₄ units. Below $T_N = 2.4$ K, three-dimensional antiferromagnetic (AFM) order sets in with an incommensurate propagation vector $\boldsymbol{\kappa} = (0, \kappa_y, 0)$ with $\kappa_y = 0.532$,¹⁵ stabilized by frustration of nearest neighbor (J_1) ferromagnetic (FM) and next-nearest neighbor (J_2) AFM exchange interactions along the chain.^{16,17} Simultaneously, an electric polarization appears along the a axis.¹⁸ In a magnetic field along the a axis, a spin-flop transition occurs at $H_a^{\text{SF}} = 2.5$ T.^{19,20} A concomitant flop of \mathbf{P} from the a to the c axis is observed for $\mathbf{H} \parallel \mathbf{a}$, while no electric polarization is reported along b irrespective of the magnetic-field direction above H_b^{SF} .²¹

Heat-capacity measurements show that the magnetic order in LiCuVO₄ develops directly from the paramagnetic *Imma* phase in a single second-order phase transition without any hysteresis within the accuracy (<5 mK) of the relaxation

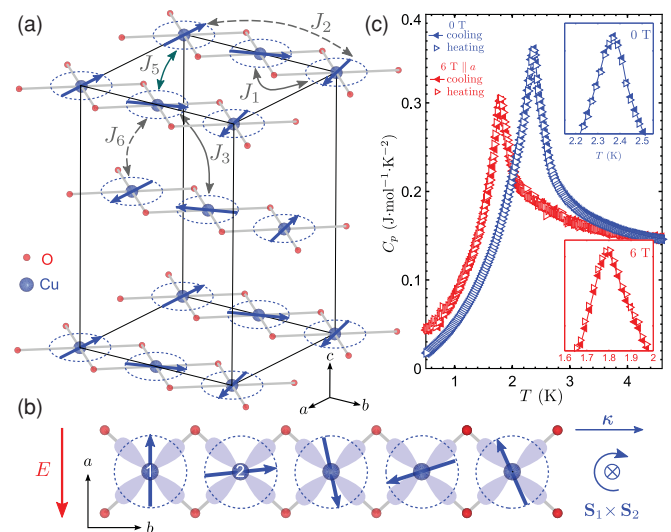


FIG. 1. (Color online) (a) Unit cell of LiCuVO₄ where only edge-sharing CuO₄ chains are shown. Solid (dashed) lines represent the ferromagnetic (antiferromagnetic) exchange interactions. (b) Isolated edge-sharing CuO₄ chain with single-hole $d_{x^2-y^2}$ orbitals and a $-im'$ cycloid. (c) Heat capacity at the magnetic transition shows absence of hysteresis between heating and cooling.

method of our Quantum Design calorimeter [Fig. 1(c)]. This indicates that symmetry breaking atomic displacements are negligible, which is also confirmed by our single-crystal neutron-diffraction measurements below T_N .

We have determined the zero-field magnetic structure of LiCuVO_4 by reanalyzing the unpolarized neutron-diffraction data of Ref. 15. We find that the ordered Cu moments lie in the ab plane forming a planar spin spiral, which propagates along the b axis. This cycloid structure can be described in terms of Fourier components of the magnetic moments at the two Cu positions as $\mathbf{m}_1^\kappa = (m_a, \pm im_b'', 0)$ and $\mathbf{m}_2^\kappa = -\mathbf{m}_1^\kappa \exp(-i\pi\kappa_y)$ with m_a and m_b'' being real and positive. The \pm sign corresponds to two possible chirality domains.

The population of these two chirality domains can be controlled by an electric field, as shown by our spherical neutron polarimetry measurements. In this technique, the directions of the incoming (\mathbf{P}_i) and outgoing (\mathbf{P}_f) neutron polarization can be chosen independently, using a so-called ‘‘cryopad’’ device.²² This device was mounted on the thermal triple-axis spectrometer IN20 at the Institut Laue-Langevin. Polarized neutrons of wave vector 2.662 \AA^{-1} were produced and analyzed by the (111) reflection of Heusler crystals as monochromator and analyzer, while second-order (unpolarized) neutrons were removed by a PG(002) filter in the scattered beam. A single crystal of LiCuVO_4 of size $1.9 \times 0.7 \times 5 \text{ mm}^3$ was aligned in the bc plane and cooled down to $T = 1.5 \text{ K}$ in a vertical electric field $E_a \simeq 45 \text{ kV/m}$ pointing in the $-a$ direction. Scans along $(0k0)$ were performed for magnetic Bragg reflections $(0, \pm\kappa', \pm\ell)$ with $\ell = 1, 3, 5$, and $\kappa' = 1 - \kappa_y = 0.47$. Introducing a Cartesian coordinate system with \hat{x} along \mathbf{Q} , \hat{y} perpendicular to \mathbf{Q} in the scattering plane, and \hat{z} perpendicular to the scattering plane, the neutron cross section for \mathbf{P}_i along \hat{y} and \mathbf{P}_f along $\pm\hat{x}$ is $\sigma_{yx, y\bar{x}} \propto \frac{1}{2}(|\mathbf{M}_{\perp\mathbf{Q}}|^2 \mp i[\mathbf{M}_{\perp\mathbf{Q}}^* \times \mathbf{M}_{\perp\mathbf{Q}}] \cdot \hat{x})$. Here, $\mathbf{M}_{\perp\mathbf{Q}} = \mathbf{Q} \times [\mathbf{M}(\mathbf{Q}) \times \mathbf{Q}]/|\mathbf{Q}|^2$ is the component of the magnetic structure factor, $\mathbf{M}(\mathbf{Q}) = \sum_j \mathbf{m}_j^\kappa \exp(i\mathbf{Q} \cdot \mathbf{r}_j)$, that is perpendicular to the wave-vector transfer $\mathbf{Q} = (h, k, \ell)$. We note that the chiral term $i[\mathbf{M}_{\perp\mathbf{Q}}^* \times \mathbf{M}_{\perp\mathbf{Q}}]$ is either parallel or antiparallel to \mathbf{Q} .

Figure 2(a) shows the resulting $\sigma_{yx, y\bar{x}}$ cross sections for the magnetic Bragg peak $(0, -\kappa', 1)$. For the cycloid with $-im_b''$ sketched in Fig. 1(b), the b component of $\mathbf{M}(\mathbf{Q})$ is negative (the dashed red arrow shows its projection $\perp \mathbf{Q}$), which implies that the chiral term $i[\mathbf{M}_{\perp\mathbf{Q}}^* \times \mathbf{M}_{\perp\mathbf{Q}}]$ in the cross section is parallel to \mathbf{Q} . Intensity should then be observed only in the $\sigma_{y\bar{x}}$ channel, which is the case. At $\mathbf{Q} = (0, \kappa', 1)$ [Fig. 2(b)], the direction of the propagation vector κ is reversed, which in turn reverses the b component of $\mathbf{M}(\mathbf{Q})$, since $\mathbf{m}_j^{-\kappa} = (\mathbf{m}_j^\kappa)^*$. The sign of the chiral term is therefore reversed, i.e., it is antiparallel to \mathbf{Q} , and intensity is observed in σ_{yx} , still corresponding to the same chirality of the cycloid ($-im_b''$). At $\mathbf{Q} = (0, \kappa', -1)$ [Fig. 2(c)], the directions of both \mathbf{Q} and κ are reversed, and the situation of Fig. 2(a) is recovered. Cooling the sample in zero electric field leads to equal intensity in the two polarization channels, which implies that both domains are equally populated. From these observations we conclude that an electric field $\mathbf{E} \parallel \mathbf{a}$ controls the chiral domain population and that the ME coupling is negative, $A < 0$, since the populated domain has $\mathbf{e}_{12} \times (\mathbf{S}_1 \times \mathbf{S}_2)$ antiparallel to \mathbf{P} (and \mathbf{E}).

To obtain more quantitative information on the magnetic structure for $\mathbf{E} \parallel \mathbf{a}$, we modeled all 36 polarized cross sections

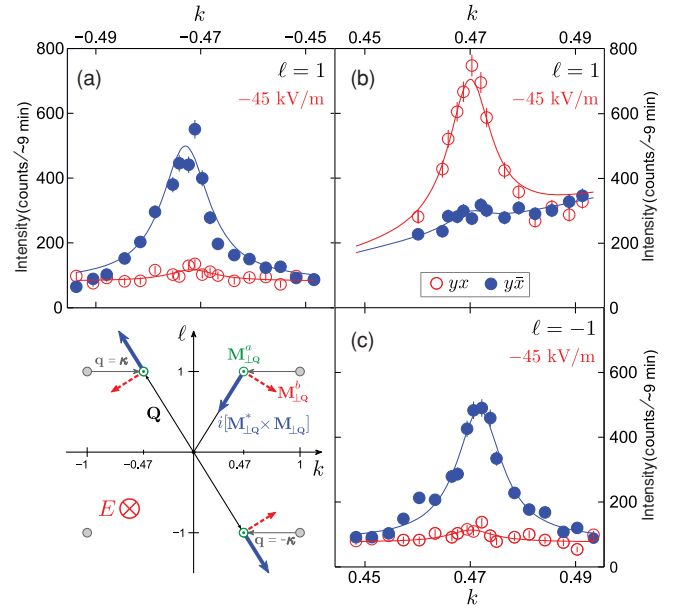


FIG. 2. (Color online) (a)–(c) Neutron polarization dependence of the magnetic reflections $(0, \pm 0.47, \pm 1)$ at $T = 1.5 \text{ K}$ with an electric field E_a directed along the $-a$ direction. The lower-left panel is a sketch of the Brillouin zone in the bc plane.

$\sigma_{\alpha\beta}$ ($\alpha, \beta = \pm x, \pm y, \pm z$) of the five magnetic Bragg peaks measured using a more general $\mathbf{m}_i^\kappa = (m_a, m_b' + im_b'', 0)$, i.e., allowing m_b to have a real component in addition to the imaginary one considered until now. A least-squares fit was performed with m_a , m_b' , m_b'' , and d_- as free parameters, where d_- is the domain population of the $-im_b''$ domain. The resulting parameters $m_b' = 0.01(5)m_a$, $m_b'' = 0.95(3)m_a$, and $d_- = 0.99(2)$ establish that the zero-field magnetic structure is a *circular* cycloid in the ab plane with a single chirality domain fully populated. A similar fit of two reflections measured with $E = 0$ gave an equal domain population, i.e., $d_- = d_+ = 0.50(0)$, which strongly supports the conclusion that full control of the cycloid chirality is achieved by applying an electric field along a .

These results are confirmed when a magnetic field \mathbf{H} is applied close to the c axis, in which case no spin-flop transition is expected or observed. In order to detect the chiral term we used the same bc -oriented sample as before with a magnetic field in the horizontal scattering plane and a vertical electric field $\mathbf{E} \parallel \mathbf{a}$. Compared to the previously described setup, we used an unpolarized incoming beam from a Si(111) monochromator but kept polarization analysis and a spin flipper in the scattered beam. In this configuration, \mathbf{P}_f is parallel or antiparallel to \mathbf{H} . The neutron polarization for a sample cooled in a positive electric field is shown in Fig. 3(b), and, following the same reasoning as for Fig. 2, corresponds to a cycloid with $+im_b''$. The sample was then warmed up to 10 K , well above T_N , and cooled down in a reversed electric field. This leads to a complete inversion of the chiral domain population [Fig. 3(c)]. Complementary measurements with $H = 3.5 \text{ T}$ exactly along the c axis corroborate these findings [see Fig. 3(d)]. From this, we conclude that the ab cycloid is stable upon application of $\mathbf{H} \parallel c$ up to at least 3.5 T and that an electric field along $\pm a$ fully controls the chirality of

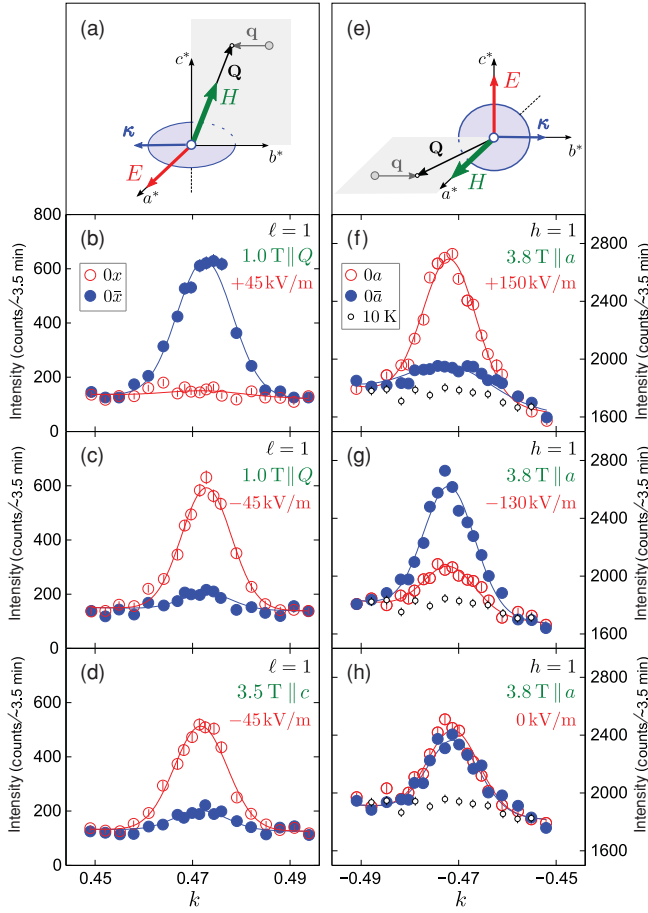


FIG. 3. (Color online) (a)–(d) Neutron polarization dependence of the magnetic reflection $(0, 0.47, 1)$ at $T = 2.1$ K with $E_a \simeq \pm 45$ kV/m and $H = 1$ T along \mathbf{Q} as sketched in (a) or $H = 3.5$ T along \mathbf{c} . (e)–(g) Similar scans for $(1, -0.47, 0)$ at $T = 1.9$ K with $E_c \neq 0$ and $H_a = 3.8$ T along \mathbf{a} as sketched in (e). The $E_c < 0$ value had to be reduced with respect to $E_c > 0$ due to electric discharges. (h) Same scans for $E = 0$. Identical results are obtained with the direction of \mathbf{H} reversed.

the cycloid. Furthermore, we find that the ME coupling is negative, $A < 0$, as in zero magnetic field.

A crucial test of the validity of the spin supercurrent model for LiCuVO_4 is to raise the magnetic field above the spin-flop field H_a^{SF} , where theory predicts a cycloid in the bc plane, which according to Ref. 14 results in a positive ME coupling, $A > 0$. Measurements were performed on a $4.5 \times 3.5 \times 1$ mm³ single crystal aligned in the ab plane and cooled down with $\mathbf{H} \parallel \mathbf{a} = 3.8$ T and $\mathbf{E} \parallel +\mathbf{c}$ as sketched in Fig. 3(e). A magnetic peak was found at $\mathbf{Q} = (1, \kappa', 0)$, which confirms the stability of the propagation vector κ for $H_a > H_a^{\text{SF}}$. As shown in Figs. 3(f)–3(h), \mathbf{P}_f changes sign when \mathbf{E} is reversed (under field-cooled conditions) and essentially vanishes for zero electric field. For an electric field $\mathbf{E} \parallel +\mathbf{c}$ ($-\mathbf{c}$) of 150 (130) kV/m, we observe a circular cycloid given by $\mathbf{m}_1^\kappa = (0, m, \pm im)$ with $+im$ ($-im$) and a domain population of $d_+ = 0.87$ ($d_- = 0.78$) [Figs. 3(f) and 3(g)], while for zero electric field an equal domain population is observed, $d_+ = 0.55(2)$ [Fig. 3(h)]. We conclude that an electric field along the c axis controls the magnetic domain population of

the spin cycloid observed above the spin-flop field, at $H_a = 3.8$ T. The chirality of the cycloid is such that the ME coupling constant A is positive for the bc -plane structure, $A > 0$.

Symmetry analysis, which is directly applicable since there is only one second-order phase transition, leads to four one-dimensional irreducible representations (IR), none of which can describe the observed ab cycloid. To proceed, we calculate the mean-field ground-state energy, $\varepsilon_{\text{gs}}(\kappa) = \sum_{\kappa} \sum_{ij} [\mathbf{S}_i(-\kappa) \mathbf{J}_{ij}(\kappa) \mathbf{S}_j(\kappa)]$, where $\mathbf{J}_{ij}(\kappa)$ is a (complex) 6×6 matrix representing the Fourier-transformed exchange interactions. Imposing the symmetry constraints of the $Imma$ space group on $\mathbf{J}_{ij}(\kappa)$ leads to cancellation of all off-diagonal terms except terms of type yz . This implies that the DMI term of type xy (D_z) is zero for every bilinear exchange path, which precludes the stabilization of an ab cycloid by DMI. A bc cycloid cannot be stabilized either by DMI, since the yz (D_x) term alternates in sign along the chain. If we impose as constraints our experimental findings that $h + l$ is odd, $m_c = 0$, and that the magnetic structure contains both m_a and m_b components, it follows from minimizing $\varepsilon_{\text{gs}}(\kappa)$ that the exchange matrix is pseudotetragonal for all dominant exchange paths defined in Ref. 16, unless there are pathological coincidences of the exchanges. The cycloid is then stabilized in the ab plane by a diagonal exchange anisotropy of easy-plane type, $|J_z| < |J_x| = |J_y|$. Imposing as maximum spin value $S = \frac{1}{2}$ on both Cu sites, we find that the general Fourier component of site 1, $\mathbf{m}_1^\kappa = (m_a, \pm [m'_b + im'_b], 0)$, is reduced to $\mathbf{m}_1^\kappa = (m, \pm im, 0)$ with m real. This corresponds to the combination of two irreducible representations with equal amplitude in quadrature and represents two degenerate perfectly circular cycloids of either rotation sense, in agreement with our experimental findings. From these mean-field considerations, we conclude that the zero-field spin-cycloid of LiCuVO_4 occurs without stabilizing DMI, driven exclusively by frustrated anisotropic diagonal (pseudotetragonal) exchange.

A magnetic field applied in the ab plane leads to a spin-flopped cycloid or helix in a plane perpendicular to the field as soon as the Zeeman energy overcomes the anisotropic diagonal exchange. Our finding of a (near) single-domain spin-flopped bc -plane cycloid for $H_a > H_a^{\text{SF}}$ and $\mathbf{E} \parallel \mathbf{c}$ with the same propagation vector as before and a chirality that depends on the sign of the electric field confirms the purely diagonal exchange scheme, and is quite distinct from the complex behavior of other materials.¹³ The anisotropy of the diagonal exchange energy calculated within mean-field theory using the spin-flop field of 2.5 T and the main exchange integrals from Ref. 16 is less than $\sim 0.5\%$. Similar energy considerations for the spin-flop field put an upper limit on the ratio of off-diagonal (yz) and diagonal exchange energy to less than 4×10^{-4} . The exchange matrix of LiCuVO_4 is hence remarkably isotropic, with diagonal anisotropic exchange being the leading (small) perturbation. This pseudotetragonal spin symmetry of the exchange matrix has its origin in the almost tetragonal symmetry of the CuO_6 octahedron and the perfectly flat edge-shared CuO_4 chains in the ab plane of LiCuVO_4 . The latter lead to a pseudotetragonal exchange matrix even in the presence of a small (orthorhombic) distortion of the bond angles away from 90° .²³

By combining our experimental results with mean-field calculations, we have shown that the formation of a ferroelectric spin cycloid in LiCuVO_4 below T_N is driven by purely diagonal frustrated anisotropic exchange without stabilizing static DMI or magnetostriction. This rules out most of the currently discussed mechanisms for FE except the spin supercurrent scenario.⁸ This purely electronic scenario has been studied for both linear Cu-O-Cu clusters of e_g electrons²⁴ and for edge-sharing CuO_4 geometry.^{14,23,25} In the latter case, SOC has been shown to generate a small symmetric exchange anisotropy²³ as well as Coulombic ring-exchange processes,^{23,25} which lead to chiral correlations and finally ME coupling.²⁵ Tetramer diagonalization and first-principles calculations of the SOC on O and Cu sites of LiCuVO_4 show that the spin supercurrent creates FE polarization in the absence of atomic displacements,

only by asymmetric orbital occupancy.¹⁴ These calculations predict the sign change of the ME constant A at the spin-flop transition for $\mathbf{H} \parallel \mathbf{a}$ that we observe experimentally.

We conclude that the purely electronic scenario of spin supercurrents is realized in LiCuVO_4 : A small symmetric exchange anisotropy is present while magnetostriction and static DMI are negligible, and the theoretical predictions of both the ratio of the electric polarizations P_a/P_c and the sign of the ME coupling in all ferroelectric phases are found in excellent agreement with experiments.

We acknowledge fruitful discussions with J. Schweizer, G. Nenert, T. Ziman, and M. E. Zhitomirsky and experimental assistance from P. Steffens, P. Chevalier, E. Bourgeat-Lami (neutrons), and G. Siegle (specific heat).

- ¹S. W. Cheong and M. Mostovoy, *Nat. Mater.* **6**, 13 (2007); Y. Tokura and S. Seki, *Adv. Mater.* **22**, 1554 (2010).
- ²T. Kimura *et al.*, *Nature (London)* **426**, 55 (2003); M. Kenzelmann, A. B. Harris, S. Jonas, C. Broholm, J. Schefer, S. B. Kim, C. L. Zhang, S. W. Cheong, O. P. Vajk, and J. W. Lynn, *Phys. Rev. Lett.* **95**, 087206 (2005); N. Aliouane, K. Schmalzl, D. Senff, A. Maljuk, K. Prokes, M. Braden, and D. N. Argyriou, *ibid.* **102**, 207205 (2009).
- ³P. G. Radaelli, L. C. Chapon, A. Daoud-Aladine, C. Vecchini, P. J. Brown, T. Chatterji, S. Park, and S. W. Cheong, *Phys. Rev. Lett.* **101**, 067205 (2008).
- ⁴Y. Yamasaki, H. Sagayama, T. Goto, M. Matsuura, K. Hirota, T. Arima, and Y. Tokura, *Phys. Rev. Lett.* **98**, 147204 (2007).
- ⁵S. Seki, Y. Yamasaki, M. Soda, M. Matsuura, K. Hirota, and Y. Tokura, *Phys. Rev. Lett.* **100**, 127201 (2008).
- ⁶I. Cabrera, M. Kenzelmann, G. Lawes, Y. Chen, W. C. Chen, R. Erwin, T. R. Gentile, J. B. Leão, J. W. Lynn, N. Rogado, R. J. Cava and C. Broholm, *Phys. Rev. Lett.* **103**, 087201 (2009).
- ⁷T. Finger, D. Senff, K. Schmalzl, W. Schmidt, L. P. Regnault, P. Becker, L. Bohaty, and M. Braden, *Phys. Rev. B* **81**, 054430 (2010).
- ⁸H. Katsura, N. Nagaosa, and A. V. Balatsky, *Phys. Rev. Lett.* **95**, 057205 (2005).
- ⁹S. Murakami, N. Nagaosa, and S. C. Zhang, *Science* **301**, 1348 (2003).
- ¹⁰M. Mostovoy, *Phys. Rev. Lett.* **96**, 067601 (2006).
- ¹¹P. G. Radaelli, C. Vecchini, L. C. Chapon, P. J. Brown, S. Park, and S. W. Cheong, *Phys. Rev. B* **79**, 020404(R) (2009).
- ¹²I. A. Sergienko and E. Dagotto, *Phys. Rev. B* **73**, 094434 (2006).
- ¹³M. Mochizuki and N. Furukawa, *Phys. Rev. Lett.* **105**, 187601 (2010).
- ¹⁴H. J. Xiang and M.-H. Whangbo, *Phys. Rev. Lett.* **99**, 257203 (2007). The sign of \mathbf{P} is clarified in Refs. 9 and 28 of H. J. Xiang, S. H. Wei, M. H. Whangbo, and J. L. F. DaSilva, *Phys. Rev. Lett.* **101**, 037209 (2008).
- ¹⁵B. J. Gibson, R. K. Kremer, A. V. Prokofiev, W. Assmus, and G. J. McIntyre, *Physica B* **350**, 253(E) (2004).
- ¹⁶M. Enderle, C. Mukherjee, B. Fåk, R. K. Kremer, J.-M. Broto, H. Rosner, S.-L. Drechsler, J. Richter, J. Malek, A. Prokofiev, W. Assmus, S. Pujol, J.-L. Raggazzoni, H. Rakoto, M. Rheinstädter, and H. M. Rønnow, *Europhys. Lett.* **70**, 237 (2005).
- ¹⁷M. Enderle, B. Fåk, H. J. Mikeska, R. K. Kremer, A. Prokofiev, and W. Assmus, *Phys. Rev. Lett.* **104**, 237207 (2010).
- ¹⁸Y. Naito, K. Sato, Y. Yasui, Y. Kobayashi, Y. Kobayashi, and M. Sato, *J. Phys. Soc. Jpn.* **76**, 023708 (2007); Y. Yasui, Y. Naito, K. Sato, T. Moyoshi, M. Sato, and K. Kakurai, *ibid.* **77**, 023712 (2008).
- ¹⁹M. G. Banks, F. Heidrich-Meisner, A. Honecker, H. Rakoto, J.-M. Broto, and R. K. Kremer, *J. Phys.: Condens. Matter* **19**, 145227 (2007).
- ²⁰N. Büttgen, H. A. Krug von Nidda, L. E. Svistov, L. A. Prozorova, A. Prokofiev, and W. Assmus, *Phys. Rev. B* **76**, 014440 (2007).
- ²¹F. Schrettle, S. Krohns, P. Lunkenheimer, J. Hemberger, N. Büttgen, H. A. Krug von Nidda, A. V. Prokofiev, and A. Loidl, *Phys. Rev. B* **77**, 144101 (2008).
- ²²P. J. Brown, J. B. Forsyth, and F. Tasset, *Proc. R. Soc. London, Ser. A* **442**, 147 (1993).
- ²³S. Tornow, O. Entin-Wohlman, and A. Aharony, *Phys. Rev. B* **60**, 10206 (1999).
- ²⁴C. Jia, S. Onoda, N. Nagaosa, and J. H. Han, *Phys. Rev. B* **76**, 144424 (2007).
- ²⁵S. Onoda and N. Nagaosa, *Phys. Rev. Lett.* **99**, 027206 (2007).